Analyst

PAPER

Cite this: *Analyst*, 2016, **141**, 4100

In situ calibration of micro-photoionization detectors in a multi-dimensional micro-gas chromatography system†

Jiwon Lee,‡[a,b] Menglian Zhou,‡[a,b] Hongbo Zhu,[a,b] Robert Nidetz,[b,c] Katsuo Kurabayashi[b,c] and Xudong Fan*[a,b]

Received 1st February 2016,
Accepted 19th April 2016

DOI: 10.1039/c6an00261g

www.rsc.org/analyst

A photoionization detector (PID) is widely used as a gas chromatography (GC) detector. By virtue of its non-destructive nature, multiple PIDs can be used in multi-dimensional GC. However, different PIDs have different responsivities towards the same chemical compound with the same concentration or mass due to different aging conditions of the PID lamps and windows. Here, we carried out a systematic study regarding the response of 5 Krypton μPIDs in a 1 × 4-channel 2-dimensional μGC system to 7 different volatile organic compounds (VOCs) with the ionization potential ranging from 8.45 eV to 10.08 eV and the concentration ranging from ~1 ng to ~2000 ng. We used one of the PIDs as the reference detector and calculated the calibration factor for each of the remaining 4 PIDs against the first PID, which we found is quite uniform regardless of the analyte, its concentration, or chromatographic peak width. Based on the above observation, we were able to quantitatively reconstruct the coeluted peaks in the first dimension using the signal obtained with a PID array in the second dimension. Our work will enable rapid and *in situ* calibration of PIDs in a GC system using a single analyte at a single concentration. It will also lead to the development of multi-channel multi-dimensional GC where multiple PIDs are employed.

Introduction

A photoionization detector (PID) is one of the most widely used gas detectors that is applicable to a variety of organic and inorganic compounds.[1] The concept of photoionization was first introduced by Lossing and Tanaka in 1956.[2] Thereafter, the first practical PID was constructed by Lovelock in 1960,[3] and further developed by Roesler, Locke, Meloan, Price, Yamane, Freeman, and other researchers.[4–10] In 1973 the PID was commercialized by HNU Systems[11] and later applied to gas chromatography (GC) by Driscoll and Clarici in 1976.[12]

In comparison with many other types of vapor detectors such as flame ionization detectors (FIDs),[13] thermal conductivity detectors (TCDs),[14] electron capture detectors (ECDs),[15] surface acoustic waves (SAWs),[16–18] optical vapor sensors,[19–26] chemicapacitors,[27,28] chemiresistors,[29] and nanoelectronic sensors,[30,31] PIDs have advantages owing to their high sensitivity, large dynamic range, compact size, low cost, and the ability to detect a wide range of vapors with no need for external gases (*e.g.*, helium used in TCDs and hydrogen/oxygen used in FIDs).[1,6,10,32–38] In particular, the non-destructive nature of PIDs allows the use of multiple PIDs for *in situ* vapor detection in multi-dimensional GC. More specifically, two-dimensional GC may use a non-destructive flow-through setting of the PID at the junction between the end of the 1st dimensional column and the entrance of the subunit consisting of the 2nd dimensional columns. Recently, μPIDs have been developed with on-chip designs, miniaturized dimensions, and small ionization chambers.[36,38–41] They have a fast response time (~0.1 s) and significantly improved sensitivity (some of which can go to the picogram or ppt level), and can readily be integrated with micro-GC (μGC) for field applications.

PIDs exhibit different responsivities toward different chemical compounds due to their different ionization potentials. Such a responsivity difference for a given PID is calibrated with isobutylene and reported as the response factor (or correction factor),[42–44] which is the ratio between the sensitivity of isobutylene to that of target compounds. Meanwhile, different PIDs may have different responsivities towards the same chemical compound with the same concentration or mass.[45] Such a difference may result from factors like different aging

[a]*Department of Biomedical Engineering, University of Michigan, 1101 Beal Avenue, Ann Arbor, Michigan 48109, USA. E-mail: xsfan@umich.edu*
[b]*Center for Wireless Integrated MicroSensing and Systems (WIMS²), University of Michigan, Ann Arbor, MI48109, USA*
[c]*Department of Mechanical Engineering, University of Michigan, 2350 Hayward, Ann Arbor, Michigan 48109, USA*
†Electronic supplementary information (ESI) available. See DOI: 10.1039/c6an00261g
‡Equal contribution.

conditions of the PID lamps (due to their finite lifetime and Krypton gas leakage) and the PID windows (caused by contamination of gas analytes, water etching, crystal solarization and the yellowing effect due to UV damage[42,46–48]). It can also be caused by the imperfect alignment between the lamp window and the microfluidic channel in the PID during assembly. The variations in the PIDs' responsivity may be detrimental to the employment of multiple PIDs in a GC system, especially in a multi-dimensional GC system.

To calibrate the difference in responsivity of different PIDs, one can always measure each PID's response to all target analytes at all anticipated concentrations (or masses). However, this method is tedious and sometimes impossible to accomplish. The easiest and most practical approach is to compare and calibrate the responses of all PIDs in a GC system with a single analyte at a given concentration. The question is whether or not the calibration factor obtained with this analyte at a given concentration can be generally applicable to other analytes of a different concentration. In this work, we carried out a systematic study regarding the response of 5 Krypton μPIDs (UV photon energy: 10.6 eV) in a 1 × 4-channel 2-dimensional μGC system to 7 different volatile organic compounds (VOCs) with the ionization potential ranging from 8.45 eV to 10.08 eV and the concentration ranging from ~1 ng to ~2000 ng. Using one of the PIDs as the reference detector, the calibration factor for each of the remaining 4 PIDs was obtained against the first PID, which we found is quite uniform regardless of the analyte, its concentration, or chromatographic peak width. Based on the above observation, we were able to quantify the coeluted peaks in the 1st dimension using the signal obtained with a PID array in the 2nd dimension. Our work will enable rapid and *in situ* calibration of PIDs in a multi-dimensional μGC system using a single analyte at a single concentration. In turn, it will also lead to the development of multi-channel multi-dimensional GC where multiple PIDs are installed.

Experimental

Materials

Benzene (>99.9%), toluene (99.5%), ethylbenzene (99.8%), heptane (99%), styrene (99.9%), chlorobenzene (99.8%), *p*-xylene (99%), and 2-heptanone (99%) were purchased from Sigma-Aldrich (St Louis, MO) and used as received. Carbopack™ B (60–80 mesh) was purchased from Supelco (Bellefonte, PA). Compressed helium gas (99.999%) was purchased from Purityplus (Detroit, MI). GC guard columns (250 μm i.d. and 380 μm o.d.) RTX®-5 ms (10 m × 250 μm i.d., 0.25 μm coating thickness), RTX®-200 (10 m × 250 μm i.d., 0.25 μm coating thickness), universal press-tight glass capillary column connectors and angled Y connectors were purchased from Restek (Bellefonte, PA). Two-port and three-port solenoid valves were purchased from Lee Company (Westbrook, CT). A diaphragm pump was purchased from Gast Manufacturing (Benton Harbor, MI). Nickel wire (0.32 mm diameter, 1.24 Ohms per m) was purchased from Lightning Vapes (Bradenton, FL). A type K thermocouple was purchased from Omega Engineering (Stamford, CT). A silicon wafer was purchased from University Wafer (Boston, MA). The PIDs were purchased from Baseline-Mocon (Lyons, CO). A 36 V AC/DC converter was purchased from TDK-Lambda Americas Inc. (National City, CA). A 24 V and a 12 V AC/DC converter and axial fans were purchased from Delta Electronics (Taipei, Taiwan). Data acquisition cards, USB-6212 (16 bits) and USB-TC01 (for thermocouple measurement), were purchased from National Instruments (Austin, TX).

μPID module construction

The μPID module used in this work was assembled with the Krypton UV lamp, the built-in lamp drive circuit and the amplifier in a commercial PID from Baseline-Mocon (Lyons, CO, P/N #043-234) as well as a home-made flow-through ionization chamber. Rather than using a serpentine microfluidic channel, which we reported previously,[39] the current simplified version of μPID shown in Fig. 1 employed a 2 cm long straight microfluidic channel created by a 380 μm gap between two p-type <100> conductive silicon wafers with a resistivity of 0.001–0.005 Ω cm and a thickness of 380 μm. The bottom and top of the microfluidic channel were covered with a Krypton UV lamp and a glass slide, respectively, which were then glued to the conductive silicon wafers with an optical epoxy. The effective UV illumination length in the channel was about 3.5 mm (*i.e.*, the diameter of the Krypton lamp window). Since the side of the microfluidic channel was made of a conductive silicon wafer, it served as a signal collection electrode in this configuration. Two copper wires were bonded to the wafers and connected to the amplifier on the commercial PID. Finally, two guard columns (250 μm i.d. and 380 μm o.d.) were inserted into the inlet and outlet of the microfluidic channel and sealed with an optical epoxy. The detailed dimensions and electrical connections of the home-made μPID are shown

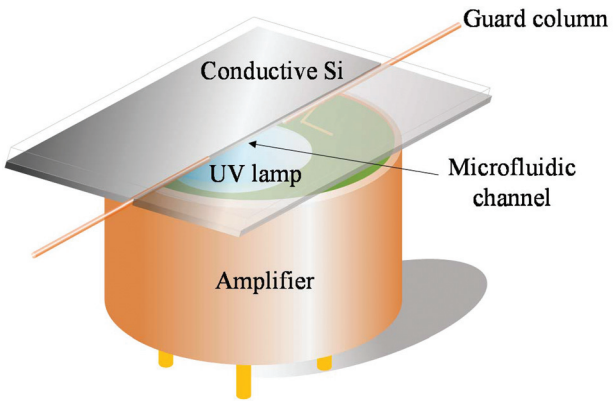

Fig. 1 Schematic of a home-made μPID with a built-in lamp drive circuit and amplifier from a commercial PID. A 380 μm wide, 380 μm tall and 2 cm long flow-through microfluidic channel was created using two conductive silicon wafers. The detailed dimensions and electrical connections are shown in Fig. S1.†

in Fig. S1.† The major difference between the current straight channel and the serpentine channel[39] is the length of the microfluidic channel under VUV illumination (3.5 mm (straight) *vs.* 2.3 cm (serpentine)), which leads to different sensitivity and hence detection limit. Nevertheless, the overall operation and flow-through principle hold for both designs. A distinct advantage of the straight channel based μPID is fabrication simplicity. It does not involve any lengthy microfabrication processes in a clean room and can be produced easily and cost-effectively.

Experimental setup

The experimental setup for PID characterization is illustrated in Fig. 2. It was arranged in a format resembling 1 × 4-channel 2-D GC so that the response of PIDs 2A–D can be calibrated against that of PID 1A. The 1st dimensional module included a microfabricated preconcentrator (μPrecon), one 10 m long RTX®-5 ms column, and PID 1A. Each of the 2nd dimensional modules included a microfabricated thermal injector (μTI), one 3 m long RTX®-200 column, and a PID to be calibrated. The flow routing system between the two separation modules consisted of three microfabricated Deans (μDeans) switches and two three-port solenoid valves to route the analytes from PID 1A to the subsequent one of PIDs in the 2nd dimension.

The μPrecon and μTI consisted of a deep-reactive-ion-etched (DRIE) silicon cavity with tapered inlet/outlet ports, an integrated platinum heater, a temperature sensor, and micro fluidic channels. Carbopack™ B granules were loaded into the cavity through a third port using a diaphragm pump, which was sealed with a silicon adhesive after loading. A small segment of the guard column was inserted into the inlet and outlet fluidic ports, and secured with an epoxy adhesive. For electrical connection, the heater and resistive temperature detector (RTD) were wire-bonded to a printed circuit board. The μPrecon and μTI were preconditioned at 300 °C for 12 hours under helium flow before use.

10 m long RTX®-5 ms and 3 m long RTX®-200 columns and a nickel wire were placed in parallel and wrapped with Teflon tape, and then coiled into a helix of 10 cm and 5 cm in diameter and 1 cm in height. A type K thermocouple was inserted into the gap between the coiled columns to monitor the column temperature in real time *via* USB-TC01. To achieve a programmed temperature ramping profile, a pulse-width-modulated signal (4.0 Hz square wave) was applied to the heater power relay *via* USB-6212. The duty cycle of the square wave was calculated by using a proportional–integral–derivative controller in the LabView™ program and updated every 0.4 s based on the set-point temperature and measured temperature at that moment.

All components, μPrecon, μTI, the heater wrapped columns and the PIDs, were mounted on a custom printed circuit board. The guard column affixed to each component was connected by using universal press-tight glass capillary column connectors or angled Y connectors. A home-made LabView™ program was developed for automated control and operation of the system, as well as the PID signal readout.

Measurement

The operation procedure was divided into two steps, *i.e.*, the first detection by PID 1A and the subsequent second detection by PIDs 2A–D.

In the first detection, the gas analyte from a Tedlar bag was drawn by using a diaphragm pump through a two port valve and adsorbed into Carbopack B inside the μPrecon. After

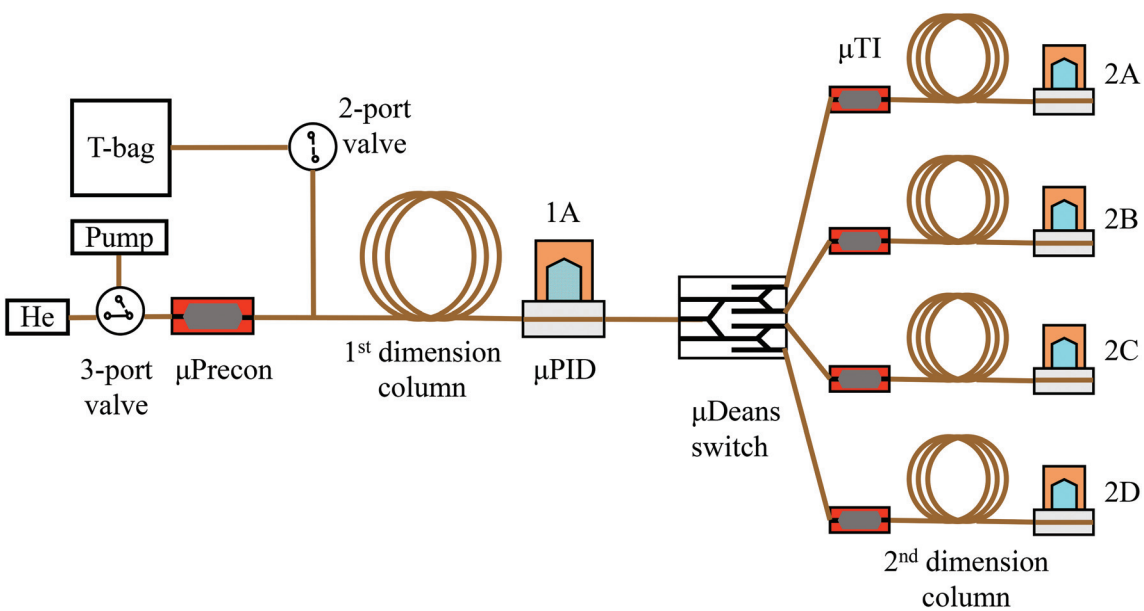

Fig. 2 Schematic of the 1 × 4-channel experimental setup to characterize and calibrate the response of 5 PIDs (1A and 2A–D). Analytes are first injected to the 1st dimensional column and detected by PID 1A. After the analytes pass through PID 1A, they are routed to one of the 2nd dimensional columns *via* micro-Deans switches and a micro-thermal injector (μTI), and finally detected by the corresponding PID.

sampling, the two valves were closed and the helium gas was flowed through a three-port valve. The μPrecon was heated up to 270 °C in 0.6 s and then kept at 250 °C for 10 s for complete thermal desorption. The analyte underwent the first separation through a RTX®-5 ms column, and was then detected by PID 1A. During the experiment, the column was heated and kept at 50 °C for 1 min and then ramped at a rate of 5 °C min^{-1}, whereas PID 1A was kept at room temperature (25 °C).

In the subsequent second detection, each of the analytes (either partial or entire amount) passing through PID 1A was routed by using the μDeans switches and trapped by using the μTI in one of the 2nd dimensional modules. Then, the μTI was heated to 270 °C in 0.6 s and then kept at 250 °C for 5 s. The analyte from the 1st dimensional module underwent the second separation through a RTX®-200 column and then was detected by one of the PIDs in this dimension (*i.e.*, PIDs 2A–D). During the experiment, all columns in the 2nd dimension were kept at 40 °C, whereas the PIDs 2A–D were kept at room temperature (25 °C).

Results and discussion

Analyte dependency

To test and calibrate the PIDs' response, individual analyte of certain mass was first placed in a Tedlar bag and then collected by the μPrecon and injected into the 1st dimensional column. After detection by PID 1A, the analyte was injected into one of the 2nd dimensional columns and detected by the corresponding PIDs (PIDs 2A–D). The same procedure was repeated until all four PIDs in the 2nd dimension were tested. Fig. 3 shows the response of all five PIDs used in the experiment (PID 1A and PIDs 2A–D) to two representative analytes (ethylbenzene and toluene). Due to the non-destructive nature of the PIDs,[49] the same amount of the analyte flowed through both PID 1A and one of the PIDs in the 2nd dimension, which allows us to compare the PID's responsivity in the 2nd dimension with that of PID 1A. For simplicity, throughout this paper we used PID 1A as the reference and calibrated the responsivity of PIDs 2A–D against that of PID 1A. From Fig. 3 we can see that the PIDs exhibit quite different responses to the same analyte of the same quantity. Such variations may result from the different aging conditions of the UV lamps and UV window, and possible misalignment of the window with respect to the microfluidic channel during μPID assembly. The calibration factor, E, for a given PID in the 2nd dimension is defined by the ratio of the peak areas, *i.e.*,

$$E_i = \frac{A_i}{A_{1A}},\ (i = 2A, 2B, 2C \text{ and } 2D) \quad (1)$$

where A_i is the peak area obtained from PIDs 2A–D and A_{1A} is the peak area obtained from PID 1A.

Using the same method described above, we calibrated the response of PIDs 2A–D to seven different analytes with the ionization potential ranging widely from 8.45 eV (*p*-xylene) to 10.08 (heptane) (see Table 1).[33] The results in Fig. 4 and Table 1 show that the calibration factor for each PID is quite uniform, although the seven analytes have quite different physical and chemical properties (such as ionization potential, vapor pressure, polarity, chromatographic peak width, *etc.*). The above result suggests that the PID calibration factor can be obtained by using a single analyte.

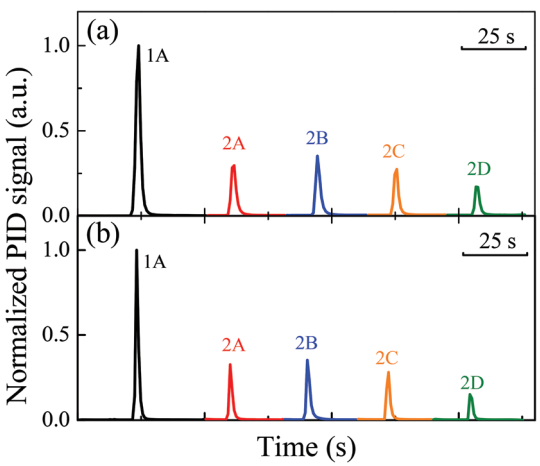

Fig. 3 The response of 5 PIDs to (a) 85 ng of ethylbenzene and (b) 92 ng of toluene. For comparison purposes, the peaks of PID 2A–D are normalized to that of PID 1A for each analyte. Additionally, all the peaks are horizontally shifted for clarity. Therefore, the *x*-axis does not represent the retention time.

Concentration dependency

In addition to the analyte dependent studies, we also investigated the concentration dependency for the PID's calibration factor. Fig. 5(a) presents the peak area of toluene obtained with PID 1A, 2A, and 2B with the injection mass ranging from 1.5 ng to 1800 ng. The peak area shows the excellent linear response to the injection mass with an R^2 of 0.9990–0.9995 in the linear regression analysis (forced zero *Y*-intercept at zero injection mass). Fig. 5(b) shows a plot of the calibration factors of PIDs 2A and 2B for each injection mass that is extracted from Fig. 5(a), showing a consistent calibration factor across an injection mass spanned over 3 orders of magnitude. The above results suggest that the calibration factor for each PID can be obtained with a single concentration (or mass) of a single analyte.

Quantitative reconstruction of the coeluted peaks

To further validate the calibration factors for the PIDs in the 2nd dimension and to demonstrate an important application of using multiple PIDs, we quantitatively reconstructed the coeluted peaks in the 1st dimensional separation using the results obtained from the PIDs in the 2nd dimension. Reconstruction of the 1st dimensional elution peaks is particularly important in comprehensive 2-D GC.[50] Since our instrument in Fig. 1 had four columns and four PIDs in the 2nd dimension, we were able to route a portion of the eluent from the 1st dimension to the 2nd dimensional columns alternately.

Table 1 Comparison of the calibration factor (standard deviation) of PIDs 2A–D to seven different analytes. The averaged calibration factor (standard deviation) is given by E_i

	Toluene	Ethyl-benzene	Styrene	Heptane	Chloro-benzene	Benzene	*p*-Xylene	E_i
IP[a]	8.82	8.76	8.47	10.08	9.07	9.25	8.49	
2A	0.343 (0.009)	0.342 (0.003)	0.336 (0.009)	0.343 (0.011)	0.343 (0.002)	0.342 (0.003)	0.349 (0.003)	0.343 (0.005)
2B	0.404 (0.007)	0.405 (0.015)	0.401 (0.013)	0.406 (0.011)	0.403 (0.013)	0.408 (0.032)	0.403 (0.013)	0.404 (0.014)
2C	0.328 (0.005)	0.332 (0.001)	0.325 (0.008)	0.318 (0.001)	0.325 (0.005)	0.323 (0.002)	0.327 (0.012)	0.325 (0.004)
2D	0.190 (0.005)	0.186 (0.008)	0.185 (0.013)	0.188 (0.004)	0.193 (0.008)	0.190 (0.002)	0.188 (0.008)	0.189 (0.006)

[a] Ionization potential (eV).

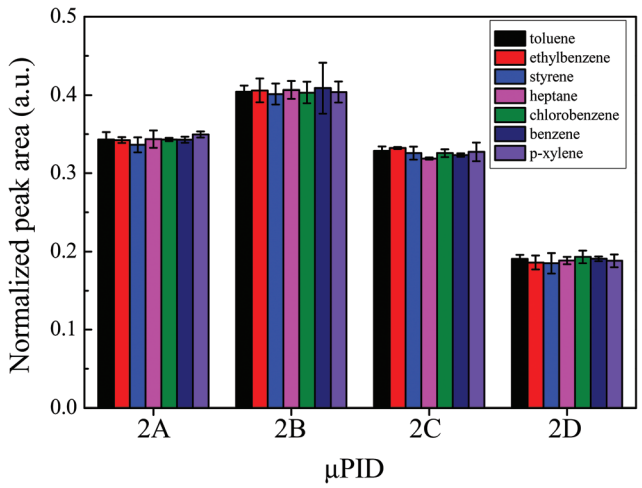

Fig. 4 Normalized peak areas obtained with PIDs 2A–D for toluene (92 ng), ethylbenzene (85 ng), styrene (90 ng), heptane (83 ng), chlorobenzene (75 ng), benzene (80 ng) and *p*-xylene (80 ng). The peak areas are normalized to that of PID 1A for each analyte. Error bars were obtained with 3 measurements. The related parameters for the analytes and PID calibration factors are given in Table 1.

In our experiment, we chose styrene and 2-heptanone as a model system. The black curve in Fig. 6(a) obtained by using PID 1A shows that these two analytes were coeluted from the 1st dimension in around 145 seconds. Fig. S2 in the ESI† illustrates how the eluent was cut and sent into the four 2nd dimensional columns by the flow routing system and subsequently detected by PIDs 2A–D. In order to reconstruct the separation peaks originally overlapped in the 1st dimension, the area under each peak in the 2nd dimension separation was computed and converted to the response of PID 1A using the calibration factor. Fig. 6(a) and (b) present the reconstructed bars for styrene and 2-heptanone, respectively. The four bars were generated from the signal obtained by using PIDs 2A–D. Each bar corresponds to a 5 s slice whose height, h, is computed as follows:

$$h_i = \frac{A_i}{E_i \times 5(\mathrm{s})}, \qquad (2)$$

where A_i is the peak area obtained by using one of the 2nd dimensional PIDs and E_i is the calibration factor for that PID (see Table 1). The total area under those bars is 2.575 Vs and 3.03 Vs for styrene and 2-heptanone, respectively. The summation of the two sets of bars is plotted in Fig. 6(c) with summed area of 5.605 Vs, which is nearly the same as 5.85 Vs obtained directly by using PID 1A (see the black curve in Fig. 6). In order to verify the reconstruction of the 1st dimension peak, Fig. 6(a) and (b) also show plots of the elution peak of styrene and 2-heptanone detected by using PID 1A when they were injected separately (see the red and blue curve in

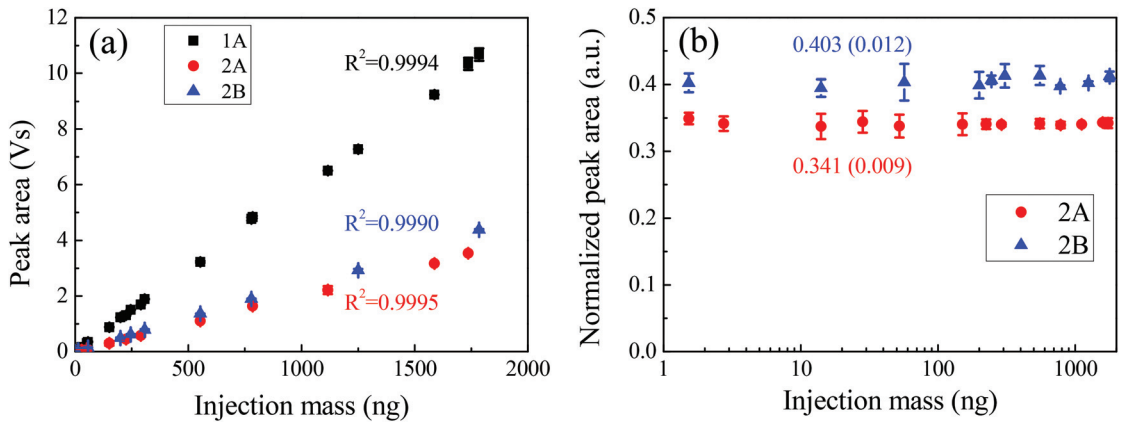

Fig. 5 (a) Peak area obtained with PIDs 1A, 2A, and 2B as a function of injection mass of toluene on the linear-linear scale. Error bars were obtained with 3 measurements. (b) The peak area of PID 2A and PID 2B normalized to that of PID 1A extracted from (a). The calibration factor for each PID averaged among different concentrations and the associated standard deviation are labeled in the figure.

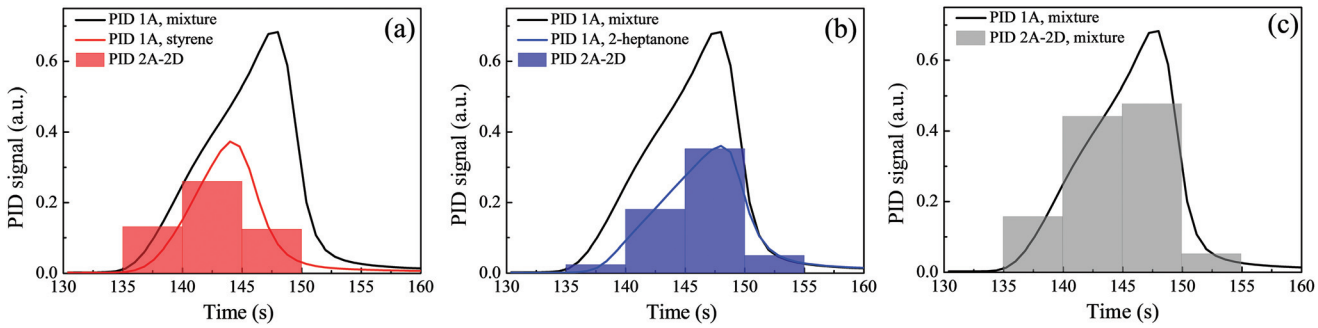

Fig. 6 (a) The coeluted peak of a mixture of styrene (285 ng) and 2-heptanone (420 ng) obtained with PID 1A (black curve). The peak reconstructed with the signals from PIDs 2A–2D for styrene (red bars). The peak of styrene obtained with PID 1A (red curve) when it was injected individually at 285 ng. (b) The coeluted peak of a mixture of styrene (285 ng) and 2-heptanone (420 ng) obtained with PID 1A (black curve). The peak reconstructed with the signals from PIDs 2A–2D for 2-heptanone (420 ng) (blue bars). The peak of 2-heptanone obtained with PID 1A (blue curve) when it was injected individually at 420 ng. (c) The coeluted peak of a mixture of styrene (285 ng) and 2-heptanone (420 ng) obtained with PID 1A (black curve). Grey bars are the summation of red and blue bars in (a) and (b). Details of routing the 1st dimension eluent to the 2nd dimension columns are illustrated in Fig. S2 in the ESI.† Details of the peak areas are given in Table 2.

Table 2 Comparison of the total area under red, blue, and grey bars obtained with PIDs 2A–2D and the peak area obtained with PID 1A

	Styrene (red)	2-Heptanone (blue)	Mixture (grey)
Bar	2.575 (Vs)	3.03 (Vs)	5.605 (Vs)
Curve	2.46 (Vs)	3.006 (Vs)	5.85 (Vs)

Fig. 6). The peak area of 2.46 Vs for styrene and 3.006 Vs for 2-heptanone matches well with the respective area obtained from the reconstructed peaks. The details of the peak areas are also given in Table 2.

Conclusions

We have investigated the responsivity of different PIDs to seven VOCs with different ionization potentials and concentrations in a 1 × 4-channel 2-D GC. The calibration factor obtained by the ratio of the peak areas for each PID was uniform regardless of the analyte and its concentration, suggesting that different PIDs can be calibrated with a single analyte with a single concentration. In addition, we demonstrated quantitative reconstruction of the coeluted peak in the 1st dimension with a PID array in the 2nd dimension. Our work will not only enable the rapid and *in situ* calibration of PIDs but also lead to the development of multi-channel multi-dimensional GC where multiple PIDs are employed.

Acknowledgements

We would like to thank the Environmental Protection Agency (83564401), the National Science Foundation (IIP-1342917) and the University of Michigan WIMS^2 Seedling Grant for financial support, and the Lurie Nanofabrication Facility for assistance in chip fabrication.

References

1 P. Verner, Photoionization detection and its applications in gas chromatography, *J. Chromatogr.*, 1984, **300**, 249–264.
2 F. P. Lossing and I. Tanaka, Photoionization as a source of ions for mass spectrometry, *J. Chem. Phys.*, 1956, **25**, 1031–1034.
3 J. E. Lovelock, A photoionization detector for gases and vapors, *Nature*, 1960, **188**, 401.
4 J. F. Roesler, Preliminary Study of Characteristics of Photoionization Detector for Gas Chromatography, *Anal. Chem.*, 1964, **36**, 1900–1903.
5 D. C. Locke and C. E. Meloan, Study of the Photoionization Detector for Gas Chromatography, *Anal. Chem.*, 1965, **37**, 389–395.
6 J. G. W. Price, D. C. Fenimore, P. G. Simmonds and A. Zlatkis, Design and operation of a photoionization detector for gas chromatography, *Anal. Chem.*, 1968, **40**, 541–547.
7 M. Yamane, A new argon ionization detector for gas chromatography, *J. Chromatogr., A*, 1962, **9**, 162–172.
8 M. Yamane, Operational mechanism and performance of a subsidiary discharge argon ionization detector, *J. Chromatogr., A*, 1963, **11**, 158–172.
9 R. R. Freeman and W. E. Wentworth, Helium photoionization detector utilizing a microwave discharge source, *Anal. Chem.*, 1971, **43**, 1987–1991.
10 N. Ostojić and Z. Šternberg, A new photoionization detector for gas chromatography, *Chromatographia*, 1974, **7**, 3–5.
11 J. N. Driscoll, Reviews of Photoionization Detection in Gas Chromatography: The First Decade, *J. Chromatogr. Sci.*, 1985, **23**, 488–492.
12 J. N. Driscoll and J. B. Clarici, Ein neuer Photoionisationsdetektor für die Gas-Chromatographie, *Chromatographia*, 1976, **9**, 567–570.
13 I. G. McWilliam and R. A. Dewar, Flame Ionization Detector for Gas Chromatography, *Nature*, 1958, **181**, 760–760.

14 D. L. Camin, R. W. King and S. D. Shawhan, Capillary Gas Chromatography Using Micro-Volume Thermal Conductivity Detectors, *Anal. Chem.*, 1964, **36**, 1175–1178.

15 M. S. Klee, Chapter 12: Detectors, in *Gas Chromatography*, ed. C. F. Poole, Elsevier, New York, 2012.

16 Q. Y. Cai and E. T. Zellers, Dual-chemiresistor GC detector employing layer-protected metal nanocluster interfaces, *Anal. Chem.*, 2002, **74**, 3533–3539.

17 H. B. Lin and J. S. Shih, Fullerene C60-cryptand coated surface acoustic wave quartz crystal sensor for organic vapors, *Sens. Actuators, B*, 2003, **92**, 243–254.

18 P. R. Lewis, R. P. Manginell, D. R. Adkins, R. J. Kottenstette, D. R. Wheeler, S. S. Sokolowski, D. E. Trudell, J. E. Byrnes, M. Okandan, J. M. Bauer, R. G. Manley and G. C. Frye-Mason, Recent advancements in the gas-phase MicroChemLab, *IEEE Sens. J.*, 2006, **6**, 784–795.

19 S. I. Shopova, I. M. White, Y. Sun, H. Zhu, X. Fan, G. Frye-Mason, A. Thompson and S.-J. Ja, On-Column Micro Gas Chromatography Detection with Capillary-Based Optical Ring Resonators, *Anal. Chem.*, 2008, **80**, 2232–2238.

20 J. Liu, Y. Sun and X. Fan, Highly versatile fiber-based optical Fabry-Pérot gas sensor, *Opt. Express*, 2009, **17**, 2731–2738.

21 J. Liu, Y. Sun, D. J. Howard, G. Frye-Mason, A. K. Thompson, S.-J. Ja, S.-K. Wang, M. Bai, H. Taub, M. Almasri and X. Fan, Fabry-Perot Cavity Sensors for Multipoint On-Column Micro Gas Chromatography Detection, *Anal. Chem.*, 2010, **82**, 4370–4375.

22 Y. Sun, J. Liu, D. J. Howard, X. Fan, G. Frye-Mason, S.-J. Ja and A. K. Thompson, Rapid tandem-column micro-gas chromatography based on optofluidic ring resonators with multi-point on-column detection, *Analyst*, 2010, **135**, 165–171.

23 K. Reddy, Y. Guo, J. Liu, W. Lee, M. K. Khaing Oo and X. Fan, Rapid, sensitive, and multiplexed on-chip optical sensors for micro-gas chromatography, *Lab Chip*, 2012, **12**, 901–905.

24 K. Reddy, J. Liu, M. K. Khaing Oo and X. Fan, Integrated Separation Columns and Fabry-Perot Sensors for Microgas Chromatography Systems, *J. Microelectromech. Syst.*, 2013, **22**, 1174–1179.

25 K. Scholten, X. Fan and E. T. Zellers, Microfabricated optofluidic ring resonator structures, *Appl. Phys. Lett.*, 2011, **99**, 141108.

26 K. Scholten, X. Fan and E. T. Zeller, A microfabricated optofluidic ring resonator for sensitive, high-speed detection of volatile organic compounds, *Lab Chip*, 2014, **14**, 3873–3880.

27 D. L. McCorkle, R. J. Warmack, S. V. Patel, T. Mlsna, S. R. Hunter and T. L. Ferrell, Ethanol vapor detection in aqueous environments using micro-capacitors and dielectric polymers, *Sens. Actuators, B*, 2005, **107**, 892–903.

28 S. V. Patel, S. T. Hobson, S. Cemalovic and T. E. Mlsna, Detection of methyl salicylate using polymer-filled chemicapacitors, *Talanta*, 2008, **76**, 872–877.

29 L. K. Wright and E. T. Zellers, A nanoparticle-coated chemiresistor array as a microscale gas chromatograph detector for explosive marker compounds: flow rate and temperature effects, *Analyst*, 2013, **138**, 6860–6868.

30 C. Y. Lee, R. Sharma, A. D. Radadia, R. I. Masel and M. S. Strano, On-Chip Micro Gas Chromatograph Enabled by a Noncovalently Functionalized Single-Walled Carbon Nanotube Sensor Array, *Angew. Chem., Int. Ed.*, 2008, **47**, 5018–5021.

31 G. S. Kulkarni, K. Reddy, Z. Zhong and X. Fan, Graphene nanoelectronic heterodyne sensor for rapid and sensitive vapour detection, *Nat. Commun.*, 2014, **5**, 4376.

32 J. E. Lovelock, A sensitive detector for gas chromatography, *J. Chromatogr., A*, 1958, **1**, 35–46.

33 A. N. Freedman, The photoionization detector: Theory, performance and application as a low-level monitor of oil vapour, *J. Chromatogr., A*, 1980, **190**, 263–273.

34 J. N. Driscoll and M. Duffy, Photoionization detector a versatile tool for environmental analysis, *Chromatography*, 1987, **2**, 21–27.

35 S. J. Edwards, A. C. Lewis, S. J. Andrews, R. T. Lidster, J. F. Hamilton and C. N. Rhodes, A compact comprehensive two-dimensional gas chromatography (GCXGC) approach for the analysis of biogenic VOCs, *Anal. Methods*, 2013, **5**, 141–150.

36 J. Sun, F. Guan, D. Cui, X. Chen, L. Zhang and J. Chen, An improved photoionization detector with a micro gas chromatography column for portable rapid gas chromatography system, *Sens. Actuators, B*, 2013, **188**, 513–518.

37 S. Narayanan, G. Rice and M. Agah, A micro-discharge photoionization detector for micro-gas chromatography, *Microchim. Acta*, 2014, **181**, 493–499.

38 M. Akbar, H. Shakeel and M. Agah, GC-on-Chip: Integrated Column and Photo Ionization Detector, *Lab Chip*, 2015, **15**, 1748–1758.

39 H. Zhu, R. Nidetz, M. Zhou, J. Lee, S. Buggaveeti, K. Kurabayashi and X. Fan, Flow-through microfluidic photoionization detectors for rapid and highly sensitive vapor detection, *Lab Chip*, 2015, **15**, 3021–3029.

40 R. P. Manginell, C. D. Mowry, A. S. Pimentel, M. A. Mangan, M. W. Moorman, E. S. Sparks, A. Allen and K. E. Achyuthan, Development of a Mesoscale Pulsed Helium Discharge Ionization Detector for Portable Gas Chromatography, *Anal. Sci.*, 2015, **31**, 1183–1188.

41 C. D. Mowry, A. S. Pimentel, E. S. Sparks, M. W. Moorman, K. E. Achyuthan and R. P. Manginell, Pulsed Discharge Helium Ionization Detector for Highly Sensitive Aquametry, *Anal. Sci.*, 2016, **32**, 177–182.

42 R. S. Inc., *The PID Handbook: Theory and applications of direct reading photoionization detectors*, San Jose, CA, 3rd edn, 2013.

43 M. L. Langhorst, Photoionization Detector Sensitivity of Organic Compounds, *J. Chromatogr. Sci.*, 1981, **19**, 98–103.

44 A. N. Freedman, Photoionization detector response, *J. Chromatogr., A*, 1982, **236**, 11–15.

45 I. Drummond, On-the-Fly Calibration of Direct Reading Photoionization Detectors, *Am. Ind. Hyg. Assoc. J.*, 1997, **58**, 820–822.

46 F. M. Peng, P. H. Xie, Y. G. Shi, J. D. Wang, W. Q. Liu and H. Y. Li, Photoionization detector for portable rapid GC, *Chromatographia*, 2007, **65**, 331–336.
47 J. N. Davenport and E. R. Adlard, Photoionization detectors for gas chromatography, *J. Chromatogr., A*, 1984, **290**, 13–32.
48 L. B. Edgett and S. C. Stotlar, Study Of Possible Solarization - Related Impurities In CaF2 And Other Fluorides, in *Southwest Conference on Optics*, 1985, pp. 134–139.
49 J. N. Driscoll, Evaluation of a new photoionization detector for organic compounds, *J. Chromatogr., A*, 1977, **134**, 49–55.
50 J. Blomberg, P. J. Schoenmakers, J. Beens and R. Tijssen, Compehensive two-dimensional gas chromatography (GC×GC) and its applicability to the characterization of complex (petrochemical) mixtures, *J. High Resolut. Chromatogr.*, 1997, **20**, 539–544.